Kaviani, A., Hofstetter, R., Rümpker, G., Weber, M. (2013): Investigation of seismic anisotropy beneath the Dead Sea fault using dense networks of broadband stations. - *Journal of Geophysical Research*, *118*, 7, 3476-3491

DOI: 10.1002/jgrb.50250

Investigation of seismic anisotropy beneath the Dead Sea fault using dense networks of broadband stations

Ayoub Kaviani,[1] Rami Hofstetter,[2] Georg Rümpker,[1] and Michael Weber[3]

Received 19 October 2012; revised 12 June 2013; accepted 12 June 2013; published 12 July 2013.

[1] Shear waveforms from core-refracted (SKS) phases recorded at 105 portable stations belonging to the DESERT and DESIRE campaigns and nine permanent broadband stations of the Israel Seismological Network are analyzed to study polarization seismic anisotropy beneath the region of the Dead Sea Transform fault in the Middle East. Shear wave splitting parameters exhibit variations with back azimuth (initial polarization) of the incoming SKS waves. The pattern of this variation is nearly constant along the strike of the fault suggesting a laterally uniform anisotropic structure beneath the Dead Sea region. The modeling of the azimuthal variations of the shear wave splitting parameters and split waveforms yields two-layered anisotropic models consisting of an upper layer with nearly N-S symmetry axis and a deeper layer with around N25°E symmetry axis. The split time is almost equally partitioned between the upper and lower layers allotting a value of 0.6–0.8 s to each layer. 2-D finite difference modeling across the southern segment of the Dead Sea Transform fault demonstrates that anisotropic structure in the strike-normal direction is relatively uniform. The Dead Sea Transform fault appears not to have a significant role in the development of the regional anisotropic fabric. The upper anisotropic layer is possibly related to a fossil fabric in the lithosphere, inherited from the Precambrian Pan-African Orogeny. The lower layer may be related to the mantle deformation due to the relative motion between the lithospheric plates and the asthenosphere and possibly affected by the local flow field due to mantle plumes as inferred by other studies.

Citation: Kaviani, A., R. Hofstetter, G. Rümpker, and M. Weber (2013), Investigation of seismic anisotropy beneath the Dead Sea fault using dense networks of broadband stations, *J. Geophys. Res. Solid Earth*, *118*, 3476–3491, doi:10.1002/jgrb.50250.

1. Introduction

[2] One key question related to continental transform faults is localization of the shear strain associated with strike-slip motion along the fault zone. The coupling between brittle deformation in the upper crust along the main continental transform plate boundaries and shearing in the ductile lower crust and upper mantle is a key issue for understanding the mechanical behavior of the continental lithosphere. The aim of this study is to address the role of the shear zone associated with the Dead Sea Transform (DST) fault system in the Middle East (Figure 1) in development of the mantle seismic anisotropy in the region. We focus our investigation on the segment along the DST extending from the Gulf of Aqaba in the south to the northern part of the Dead Sea Basin (DSB) in the north. The DST is a ~1100 km long sinistral strike-slip plate boundary that separates the Arabian plate from the Sinai subplate [e.g., *Freund et al*., 1970; *Ben-Menahem et al*., 1976; *Garfunkel*, 1981]. The DST has accommodated ~105 km of the differential left-lateral motion since the Early Miocene and is interconnected by a series of en echelon left-lateral over-stepping pull-apart basins [e.g., *Quennell*, 1958; *Bartov et al*., 1980; *Garfunkel*, 1981; *Garfunkel and Ben-Avraham*, 1996; *Ben-Avraham et al*., 2008], of which the most prominent is the Dead Sea Basin in the central segment of the DST. It cuts through a continental area that was formed by the Proterozoic Pan-African Orogeny and has remained a stable platform from the Cambrian through the Paleogene. The strike of the fault changes from an NNE-SSW direction on the southern segment in the region of Wadi Arava, to a more northerly direction on the northern segment in the region of Jordan Valley (Figure 1). GPS data suggest that the relative motion between the Arabian plate and Sinai subplate occurs at a relatively slow rate of 3.1–5.4 mm/yr in different parts of the Dead Sea Transform fault [*Wdowinski et al*., 2004; *Le Beon et al*., 2008; *Mahmoud et al*., 2005; *al Tarazi et al*., 2011; *Sadeh et al*., 2012].

[3] Analysis of seismic anisotropy can be used to document deformation and flow processes in the crust and upper mantle [e.g., *Crampin*, 1978, 1987; *Leary et al*., 1990; *Silver*, 1996; *Savage*, 1999; *Long and Silver*, 2009]. Tectonic stress and flow can generate pervasive fabrics in upper mantle through crystal lattice preferred orientation of rock-forming minerals, mainly

Additional supporting information may be found in the online version of this article.

[1]Geophysics Section Institute of Geosciences, Goethe-University Frankfurt, Frankfurt, Germany.
[2]Seismology Division, Geophysical Institute of Israel, Lod, Israel.
[3]Deutsches GeoForschungsZentrum, Potsdam, Germany.

Corresponding author: A. Kaviani, Geophysics Section, Institute of Geosciences, Goethe-University Frankfurt, Altenhoeferallee 1, Frankfurt DE-60438, Germany. (Kaviani@geophysik.uni-frankfurt.de)

2169-9313/13/10.1002/jgrb.50250

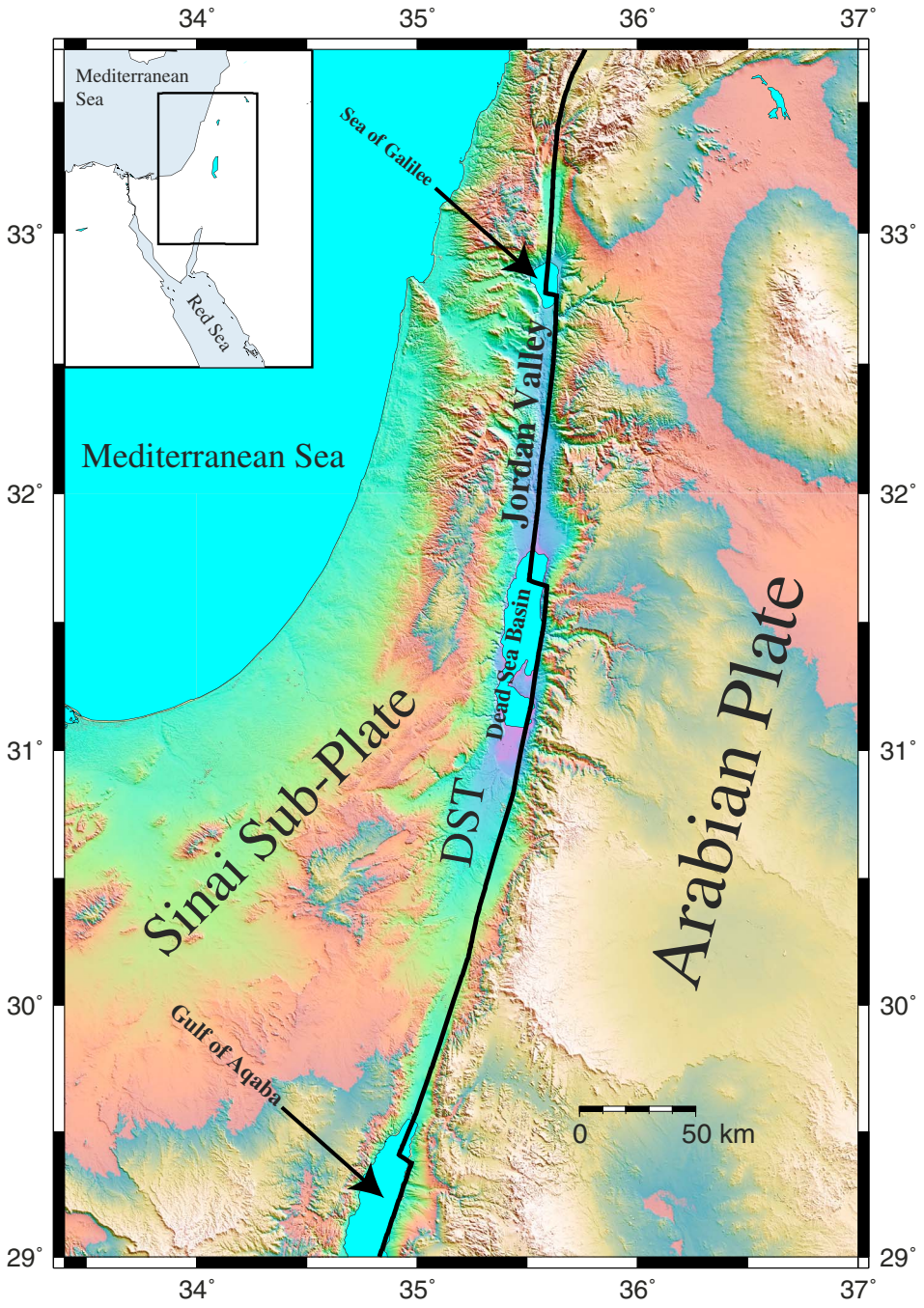

Figure 1. Topographic map of the Dead Sea Fault (shown schematically) and adjacent regions. The Dead Sea Transform fault extends as an N-S distinct physiographic feature on the map.

olivine. This preferred orientation, in turn, results in bulk anisotropy in the mantle that affects the propagation of seismic waves and imprints specific signatures on seismic records. An extensively used diagnostic of seismic anisotropy is the splitting of shear waves upon their passage through an anisotropic region of the Earth. A shear wave propagating through such regions splits into two orthogonally polarized quasi-shear waves that then travel with different velocities, leaving two pulses on the horizontal seismograms when rotated appropriately. One component of these split shear waves has polarization parallel to the fast axis of the medium, and the other component is polarized in the slow direction. As a measure of anisotropy, we quantify the polarization direction of the fast horizontal component (Φ) and the delay time (δt) accumulated between the fast and slow components on the split seismograms. The fast direction estimated by splitting analysis represents the horizontal projection of the symmetry axis of anisotropy; the delay time is a function of both the strength of anisotropy and the path length traveled by the seismic wave in the anisotropic medium.

[4] Previous seismic anisotropy studies in the Dead Sea region revealed average one-layer models with N-S fast symmetry axis and delay times between 1.0 and 1.5 s [*Schmid et al.*, 2004; *Kaviani et al.*, 2011] or two-layer models with delay times less than 1.0 s assigned to each layer and NE-

SW fast symmetry axes in the deeper layer and N-S to NNW-SSE fast symmetry azimuths in the upper layer [*Rümpker et al*., 2003; *Ryberg et al*., 2005; *Levin et al*., 2006]. Two large international multidisciplinary campaigns, known as DESERT and DESIRE have been conducted in the region aimed at studying the crustal and mantle structure on different scales beneath the Dead Sea Transform fault. Receiver function analysis [*Hofstetter and Bock*, 2004; *Mohsen et al*., 2005; *Mohsen et al*., 2011] and controlled-source seismic studies [*Mechie et al*., 2005; *ten Brink et al*., 2006; *Mechie et al*., 2009] revealed that the crust-mantle boundary (Moho) increases steadily from ~26 km at the Mediterranean coast in the west to ~39 km under the Jordan highlands. The same investigations showed that the lack of a strong uplift of the Moho beneath the surface trace of the DST precludes the hypothesis of a potential extensional regime across the DST. By surface wave analysis, *Laske et al*. [2008] showed that the upper mantle beneath the Dead Sea region has lower *S* wave seismic velocity than the standard reference model PREM. These authors relate the low-velocity structure to elevated temperatures presumably connected to rifting processes in the Red Sea. On the other hand, no significant *P* wave velocity anomalies were observed through the tomographic inversion of teleseismic *P* wave travel times recorded at seismic stations of the permanent networks of Israel and Jordan [*Hofstetter et al*., 2000] and the DESERT portable stations [*Koulakov et al*., 2006]. The same study did not observe any reliable evidence for an effect of the DST on the upper-mantle structure. The S-receiver function studies by *Mohsen et al*. [2006] unraveled the presence of a relatively thin mantle lid (~70km) in the east of the DST thickening gradually to ~80 km near the Mediterranean cost.

[5] *Rümpker et al*. [2003] and *Ryberg et al*. [2005] used waveform modeling of shear wave splitting observations from a single event along a dense profile of short-period stations across the southern DST to investigate the lateral and vertical variations in anisotropic structure beneath the array of stations. Since their observation was performed from a single back azimuth, they used frequency dependence and lateral variations of measured splitting parameters to constrain both the vertical and lateral dimensions of the anisotropic domains in their models. They tested a large variety of models that included lateral variations in anisotropic structure both in the crust and upper mantle. Their models include one layer of anisotropy in the crust and the upper mantle. The upper-mantle layer of their best fit models bears a narrow ~20 km wide vertical anisotropic zone beneath the DST with horizontal symmetry axes of 22°–26°. In order to account for short-scale lateral variations in the shear wave splitting observations, they assumed highly anisotropic domains in the crust. However, *Kaviani et al*. [2011], using a dense network of broadband seismic stations farther north of this profile across the DSB, showed that strong shallow isotropic velocity variations due to sedimentary basins can also have a significant impact on the SKS observations. The observations by *Kaviani et al*. [2011] also revealed that short-scale strong variations of the splitting parameters across the basin can obscure any signature of deeper anisotropy structures and prevent detailed investigation of mantle fabric. Modeling by *Kaviani et al*. [2011] has also shown that the small aperture of the network does not allow for further investigation of the lateral variations in the mantle anisotropic fabric beneath that segment of the DST.

[6] *Levin et al*. [2006] used seismic data from four permanent and one temporary seismic station to probe seismic anisotropy beneath the Dead Sea region by analysis of shear wave splitting of core-refracted phases. By observing remarkable azimuthal variations of splitting parameters at all the stations, they noted that the pattern of the azimuthal variations is very similar at all stations regardless of their locations relative to the surface trace of the DST. They concluded that the general anisotropic structure beneath the Dead Sea region must be uniform. They interpret the observed patterns of shear wave splitting in terms of one- and two-layer models. Their one-layer models exhibit fast axes oriented 12°–19° east of north. Their two-layer models are very similar beneath all stations exhibiting an upper layer with a nearly N-S fast axis and split time of ~1 s. The lower layer was characterized by a weaker split times and NE-SW fast polarization directions ranging between 30 and 80°. *Levin et al*. [2006] concluded that the lower layer in their models appears to be related to regional deformation due to the differential motion between the lithospheric plate and underlying mantle asthenosphere. The fast polarization direction in the upper layer is subparallel to the transcurrent motion along the Dead Sea Transform fault but also consistent with the orientation of the mantle seismic anisotropy observed in the Arabian shield away from the DST [*Hansen et al*., 2006]. This observation has led *Levin et al*. [2006] to conclude that the effect of the DST on the development of seismic anisotropy fabric in the upper mantle is probably negligible.

[7] Though the previous studies have tested numerous models of anisotropy in the Dead Sea region, the question of whether the transcurrent motion along the DST has a significant effect on the mantle fabric remains poorly understood. The combination of the seismic data sets from the dense temporary networks of the DESERT and DESIRE projects and data from the permanent stations of Israel and Jordan have provided a unique opportunity with an unprecedented spatial coverage that allows for testing different models of seismic anisotropy with lateral and depth variations along and across the DST.

[8] In this report, we focus on the analysis and modeling of seismic shear wave data from the DESIRE and DESERT temporary deployments along the DST in conjunction with the permanent broadband stations of Israel Seismic Network (ISN). This is an unprecedented data set from such dense seismological networks including 114 stations that span the along-strike and lateral extent of the Dead Sea Transform fault. We test different models of depth-dependent anisotropy structures and examine lateral variations in anisotropy at depth in order to verify the possible contribution of the DST shear zone to the mantle fabric.

2. Data and Analysis

[9] We use seismic shear waveforms from core-refracted phases (SKS, SKKS, and PKS, hereinafter referred to as *KS) recorded at 37 and 68 stations of the portable networks of DESERT and DESIRE campaigns, operating from April 2000 to June 2001 and from October 2006 to April 2008, respectively. In addition, we have included recordings from nine permanent broadband stations of the ISN. The seismic data from the permanent stations improve the azimuthal coverage and help to characterize the complexities of the

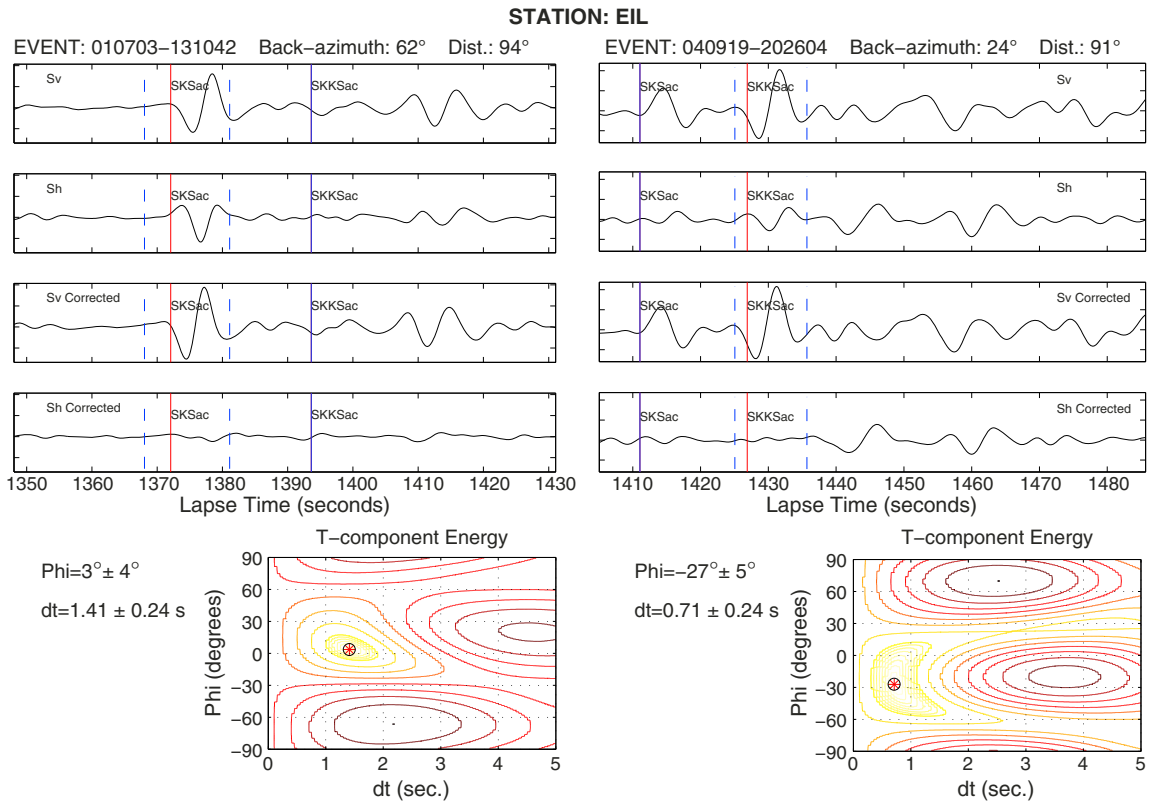

Figure 2. Two examples of the splitting analysis at station EIL from two different back azimuths. (top) The radial and tangential seismograms (before and after removal of splitting) and (bottom) the transverse component energy diagrams.

anisotropic medium. We analyzed 3683 seismograms from 707 events with magnitude 5.8 or greater at epicentral distances 87°–144°. A band-pass filtering between 0.05 and 0.25 Hz is applied to all seismograms before splitting analysis. We use both cross correlation [*Bowman and Ando*, 1987] and transverse component energy minimization [*Silver and Chan*, 1991] methods to estimate the individual splitting parameters Φ and δt. For the majority of incoming polarizations (back azimuths), only those measurements for which the splitting parameters estimated by both methods agree within the range of errors are taken as reliable. On the other hand, *Wüstefeld and Bokelmann* [2007] showed that, when the incoming polarization is very close to a null direction, the cross-correlation method yields delay-time estimates that are very low and fast directions that are nearly 45° off the true fast direction. In a multilayer case, the null directions correspond to incoming polarization directions for which the splitting parameters exhibit very rapid variations [*Silver and Savage*, 1994]. Therefore, when the splitting parameters estimated by the two methods do not agree and the incoming polarization is very close to a null direction, we select the estimate given by the method of transverse-component minimization. The quality of splitting measurement (good, fair or poor) is assessed according to the following criteria: (1) the signal-to-noise ratio of the initial *KS waveforms, (2) the ratio of the energy on the corrected radial component to that on the transverse component (>3), (3) the maximum cross correlation between the fast and slow components (>0.90), (4) the linearity of the particle motion of the corrected horizontal components, and (5) the error bars of the estimated splitting parameters (<0.3 s for δt and <30° for Φ). Some of our measurements are recognized as "null" measurements with negligible energy on the transverse component. This can happen when the net anisotropy beneath the station is too weak to generate any splitting or when the initial polarization of the shear wave is either parallel or perpendicular to the fast direction of the anisotropic medium [*Silver*, 1996; *Savage*, 1999; *Long and Silver*, 2009]. To distinguish these two possibilities, splitting measurements are often obtained for a range of different initial polarizations (back azimuths). In the case of depth-dependent or multilayered anisotropy, the energy on the transverse component never reaches zero [*Silver and Savage*, 1994; *Rümpker and Silver*, 1998]. We take a measurement to be "null" when there is little energy on the uncorrected transverse component and the initial particle motion is nearly linear [*Silver and Chan*, 1991]. In this case, the best recovered pair of splitting parameters lies in the "null" region on the energy diagram of the grid search using the transverse minimization method, where the contours are elongated along the δt axis giving large error bars for the estimated delay times [*Silver and Chan*, 1991]. The cross-correlation method also yields negligible delay time for "null" azimuths.

[10] Only measurements that pass the good and fair quality criteria are used for subsequent analysis. In total, we obtained 594 splitting measurements (431, 79, and 84 from stations of the DESIRE, DESERT, and ISN networks, respectively); 188 of those were classified as "null" measurements, mostly for azimuths 0°–20° (modulo 90). The whole set of the splitting measurements at all stations is given in Table S1–S3. Figure 2 presents two examples of splitting analysis at station

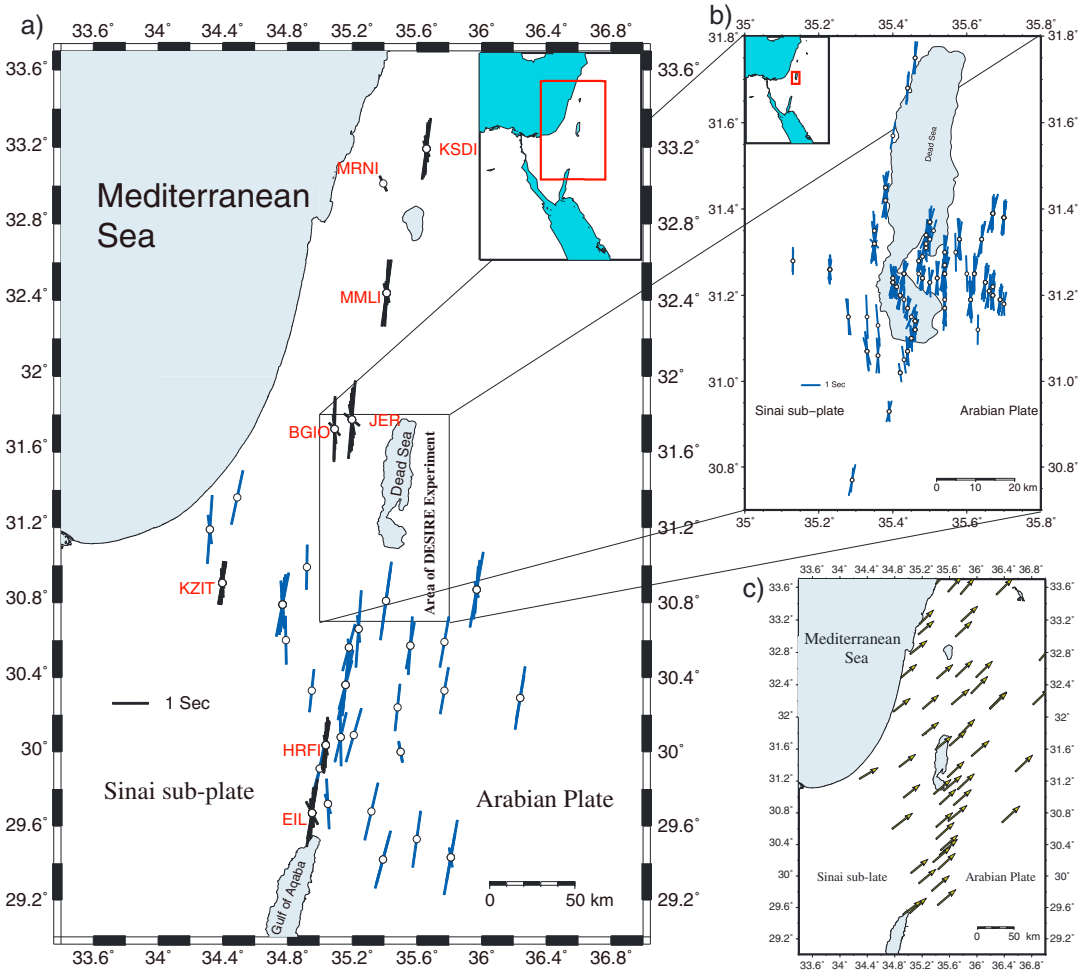

Figure 3. (a) The individual non-null splitting measurements at the DESERT temporary (blue bars) and ISN permanent (black bars) stations. The length of the bars is scaled proportional to the associated delay times. (b) The same for the DESIRE stations, the map scale is larger for the individual points to be visible. (c) Geodetic displacement map at GPS stations in the Dead Sea region in the ITRF2005 no-net-rotation reference frame [*al Tarazi et al.*, 2011].

EIL which are indicative of the azimuthal variations in the splitting parameters. The SKS waveforms used in these examples are from two events at back azimuths of 24° and 62° and result in differing splitting parameters at station EIL. The azimuthal variation in splitting parameters at station EIL implies a complex structure of anisotropy beneath this station (see section 3.2).

3. Results

3.1. Map of Individual Splitting Measurements

[11] Figure 3a shows the complete set of individual splitting parameters measured at stations of DESERT, DESIRE, and ISN. Each measurement is shown with a bar (blue and black for temporary and permanent stations, respectively) oriented in its fast direction and scaled proportional to the respective delay time. The names of the permanent stations are also shown for later reference in the following sections. The individual measurements at the DESIRE dense network are shown separately in Figure 3b on a larger scale. In Figure 3c, we depict the geodetic horizontal displacement vectors in the ITRF2005 no-net-rotation reference frame measured at a dense network of GPS stations in the Dead Sea region [*al Tarazi et al.*, 2011]. These vectors represent the "absolute" motion of the lithospheric plates relative to the underlying asthenosphere in the given reference frame. Our observed fast directions demonstrate no correlation with these horizontal displacement vectors, indicating that the anisotropy beneath the Dead Sea region cannot be explained by a simple model of merely large-scale asthenospheric flow associated with the relative movement between lithosphere and asthenosphere.

3.2. Back Azimuthal Variations in Splitting Parameters

[12] Back azimuthal variations of splitting parameters are a valuable diagnostic for depth-dependent anisotropy. In the case of multiple anisotropic layers with horizontal symmetry axes, the splitting parameters exhibit a $\pi/2$ periodicity in both Φ and δt [*Silver and Savage*, 1994; *Rümpker and Silver*, 1998]. To verify the azimuthal variations in detail, we use the non-null splitting parameters observed at the DESERT and ISN stations. The splitting parameters obtained for stations of the DESIRE network are given in *Kaviani et al.* [2011]. They show that the sedimentary fill of the Dead Sea

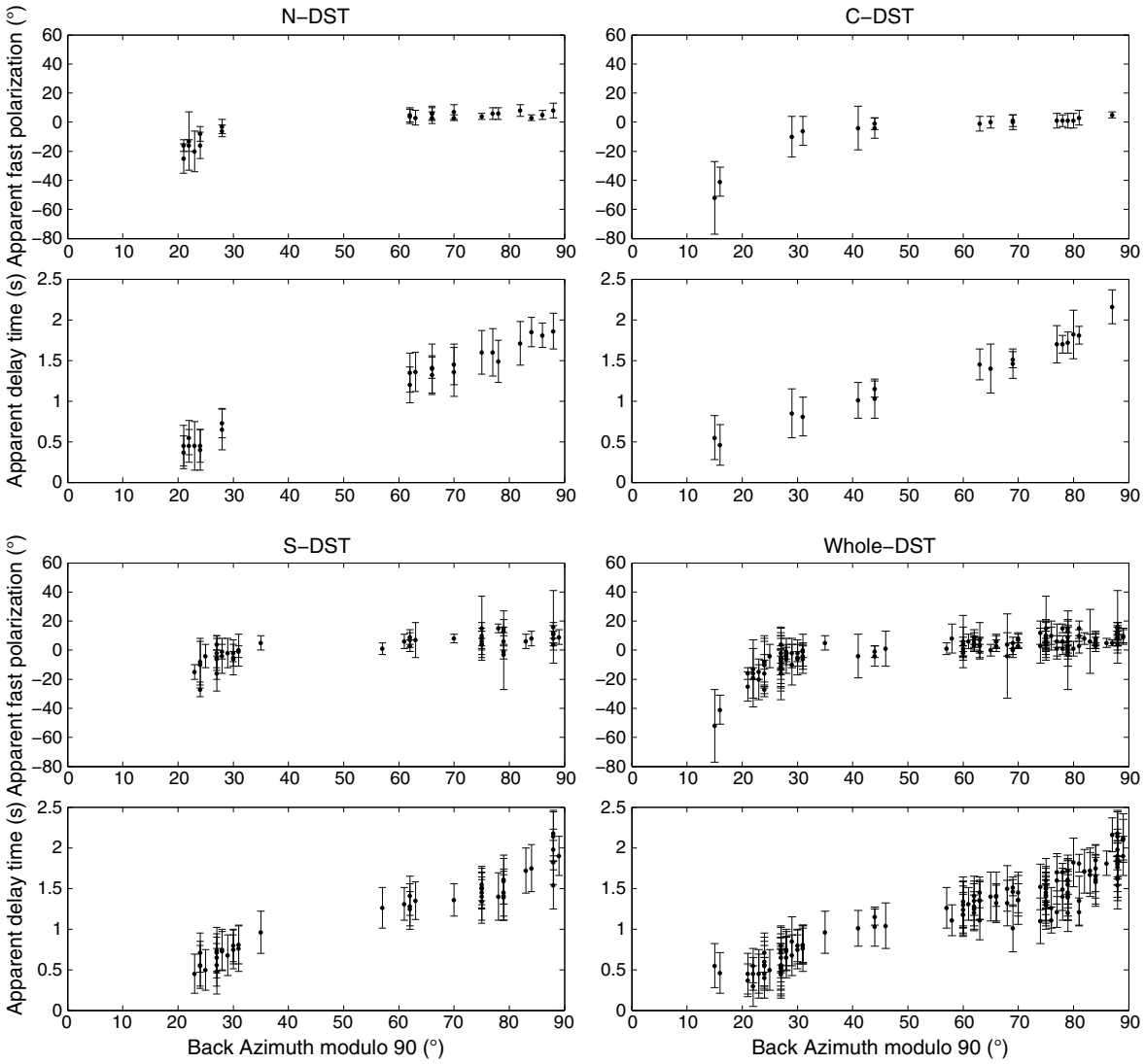

Figure 4. Variations of the apparent splitting parameters versus back azimuth modulo 90 observed at the DESERT and ISN stations along the DST. The stations are grouped regarding to their geographic location along the DST.

Basin has a strong effect on the observed splitting parameters, which also implies that depth variations of anisotropy are difficult to access at these stations. The corresponding splitting data are therefore omitted from the following analysis of the azimuthal variations of the splitting parameters. We categorized the DESERT and ISN stations in three groups according to their geographical coordinates along the DST. The first group consists of the two permanent stations EIL and HRFI together with temporary stations of the DESERT network in the vicinity of the southern segment of the DST (Figure 3a). The second group includes the two permanent stations JER and BGIO in the vicinity of the central segment of the DST, west of the DSB. The third group comprises the northernmost permanent stations KSDI, MMLI and MRNI. In Figure S1 (a-c) (supporting information) we present the azimuthal variations of non-null splitting parameters measured in the groups of stations as mentioned above. The splitting parameters exhibit systematic variations with back azimuth, where the fast polarizations vary between −52° and 16° and the delay times vary between 0.4 and 2.2 seconds. We observe similar patterns of the back azimuthal variations in the splitting parameters in all groups reflecting the similarity in anisotropic structure at depth along the DST. Motivated by this similarity, we further compile a fourth group comprising all observed splitting parameters of the combination of the DESERT temporary and ISN permanent stations along the DST. The apparent splitting parameters measured at all the DESERT and ISN stations are plotted versus back azimuth in Figure S1–d. The data show little scatter though the stations are located in different distances away from and along the DST. The splitting parameters are shown in Figure S1 as a function of back azimuth to demonstrate the azimuthal distribution of our observations and the systematic variations of the splitting parameters. In Figure 4, we present the measurements as function of back azimuth modulo $\pi/2$ to better demonstrate the $\pi/2$ periodicity of the splitting parameters.

Table 1. Two-Layer Models Obtained From the Modeling of Azimuthal Variations in the Splitting Parameters for the Three Groups of Stations and the Whole Set of the DESERT and ISN Stations Along the DST[a]

Region	Lower Layer		Upper Layer		Misfit Errors		Total Variance
	Φ (°)	δt (s)	Φ (°)	δt (s)	Φ (°)	δt (s)	
Northern DST model 1	25	0.8	−8	0.6	3.3	0.07	0.8868
Northern DST model 2	30	0.6	−3	0.8	3.3	0.07	0.8869
Northern DST model 3	38	0.5	1	1.0	3.3	0.07	0.9197
Central DST model 1	26	0.7	−10	0.7	1.2	0.04	0.3742
Central DST model 2	24	0.8	−13	0.7	1.2	0.04	0.3887
Central DST model 3	32	0.6	−7	0.9	1.2	0.04	0.4053
Southern DST model 1	26	0.8	−4	0.6	2.4	0.04	0.4926
Southern DST model 2	29	0.6	−1	0.7	2.4	0.04	0.4928
Southern DST model 3	32	0.6	1	0.8	2.4	0.04	0.4985
Whole DST model 1	26	0.6	−6	0.7	4.1	0.14	1.1919
Whole DST model 2	30	0.6	−4	0.8	4.1	0.14	1.2014
Whole DST model 3	30	0.6	−10	0.7	6.9	0.15	1.6424

[a]Total variance is the value of the penalty function for the given set of model parameters.

3.3. Modeling Back Azimuthal Variations

3.3.1. Inversion of Splitting Parameters

[13] The well-developed π/2 azimuthal periodicity of the splitting parameters motivated us to seek optimum models of depth-dependent anisotropy that best explain these variations. In our approach, we allow for layered anisotropy models with horizontal symmetry axes and perform a grid search over model parameters (delay time and fast symmetry axis in each layer). The theoretical apparent splitting parameters as functions of initial polarization are calculated using the formulations provided by *Silver and Savage* [1994] and *Rümpker and Silver* [1998]. The penalty function is defined as

$$F(\phi_1, \delta t_1, \phi_2, \delta t_2) = \left(\frac{1}{\sigma_\varphi}\right)\sqrt{\frac{\sum_{i=1}^{N} \left\|\phi_i^{obs} - \phi_i^{cal}\right\|^2}{N}} + \left(\frac{1}{\sigma_{\delta t}}\right)\sqrt{\frac{\sum_{i=1}^{N} \left\|\delta t_i^{obs} - \delta t_i^{cal}\right\|^2}{N}},$$

where N is the number of the observed splitting pairs, and σ is the average standard deviation of the observed Φ and δt, respectively. However, theoretical studies unveiled that for noisy and unevenly sampled data, there is a wide range of models that can explain the observed azimuthal patterns within the confidence region of the penalty function [*Silver and Savage*, 1994; *Rümpker and Silver*, 1998; *Hartog and Schwartz*, 2001]. Even for a two-layer model consisting of four model parameters (fast directions and delay times of the two layers), there is no unique model that best explains the shear wave observations. To mitigate the effect of this nonuniqueness, we follow a two-step grid search approach. We first use a simplified three-parameter anisotropic model as given in *Rümpker and Silver* [1998] to calculate the theoretical variation of the apparent splitting parameters versus initial polarizations. The model parameters are the fast directions at the top and bottom of the anisotropic zone and the effective delay time. These three-parameter models do indeed provide a unique set of parameters. We perform a grid search over the three model parameters by allowing for variations in fast axis between 0° and 180° and in effective delay time between 0 and 4 s. In the second step, we invert for the four parameters of a two-layer anisotropic model [*Silver and Savage*, 1994] while the fast directions in the upper and lower layers are confined to vary only around the values already estimated in the first step. Even using this two-step procedure, we observe that for each group of stations, we obtain distinct models that explain the variance of the splitting parameters in the range of the confidence interval of the penalty function. For each group, corresponding to the southern, central, and northern segment of the DST, as well as the whole data set, we obtain three distinct models that best explain the observed azimuthal pattern of the apparent splitting parameters. The three selected models for each group are shown in Table 1. The three selected models for each group are those giving the three smallest values of the penalty function F. The selected models are all similar in the sense that they consist of an upper layer with a nearly N-S oriented fast symmetry axis and a lower layer with a NE-SW oriented fast symmetry axis. The split times in the upper and lower layers in all models are relatively small and vary between 0.5 and 1.0 s. These small delay times are distributed between the upper and lower layers yielding different models. The theoretical predictions of apparent splitting parameters from the selected models for each group of stations (Table 1) are shown in Figure 5 along with the observations. As Figure 5 illustrates, the theoretical curves of the apparent splitting parameters from the selected models are practically identical and difficult to discriminate. Although the three best models for each group resemble each other, the implication of each model is different depending on the exact value of the delay times and fast symmetry axes assigned to each anisotropic layer. In order to select one model for each group (amongst the three best fit models of the group) that can be used as basis for a tectonic interpretation of the study area, we need to consider some other independent information that helps in deciding which model is most compatible. In regions of continental transform faults, one may expect the fast symmetry axis of anisotropy to be aligned parallel to the strike of the fault system, as simple shearing along the fault can produce pervasive anisotropic fabrics through the creation of subvertical foliation planes with horizontal lineation [e.g., *Tommasi et al.*, 1999; *Vauchez et al.*, 2012]. This mechanism has been shown to be effective in the San Andreas Fault (SAF) system [e.g., *Ozalaybey and Savage*, 1995; *Hartog and Schwartz*, 2001; *Polet and Kanamori*, 2002; *Bonnin et al.*, 2010]. In the case of the Dead Sea Transform fault system, we note, however, that the azimuthal variations in apparent splitting parameters exhibit very similar patterns along the strike of the DST while the strike of the fault system changes from an azimuth of ~20° in the south to a nearly N-S direction in the north. This may suggest that the symmetry axes of the layered anisotropic models are not directly related to the DST fault system. Nevertheless, we may verify this hypothesis by confining the fast direction in either the upper or lower layer to be parallel to the strike of the fault. This may be assumed for the southern segment of the DST, where the deformation along the fault may occur in a simple shear regime producing a fault parallel fabric. In the northern segment of the DST, however, the deformation is in a transpressive regime [*Garfunkel*, 1981] that can produce more complicated fabrics. In the central segment, where the over-stepping has led to the

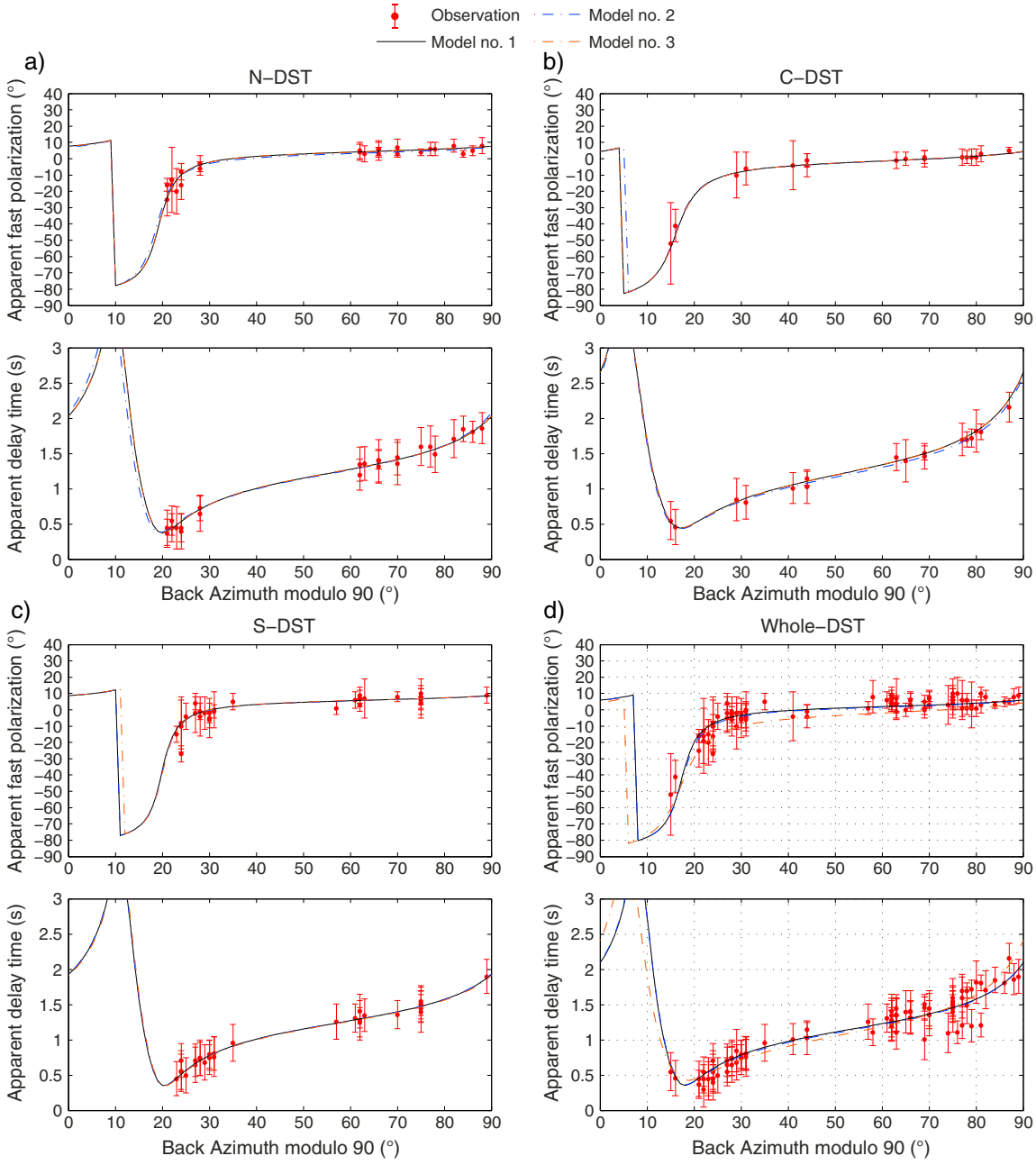

Figure 5. Theoretical predictions of apparent splitting parameters versus the initial polarization modulo 90 from the selected best fit two-layer models obtained for the southern, central, and northern segment of DST and the whole set of the DESERT and ISN stations. The model specifications are given in Table 1. The theoretical curves from the best fit models in each group are visually indistinguishable from each other indicating the nonuniqueness of the inversion results.

formation of the DSB, the anisotropic structure may be more complex [*Garfunkel and Ben-Avraham*, 1996]. We therefore attempt to find two-layer models for the southern segment of the DST by constraining the fast axis in the upper or lower layer to vary only around the general trend of the surface trace of the DST in the region, which we take to be 19° ± 3°. The two models with fixed fast symmetry axis in upper or lower layer that best fit the observed azimuthal pattern of the splitting parameters are listed in Table 2. The corresponding theoretical curves of the apparent splitting parameters are also shown in Figure 6. These models, although uniquely determined, do not provide a better explanation of the observed splitting parameters than do the above mentioned selected models. As illustrated in Figure 6 and shown by the values of the misfit errors in Table 2, there is no unique two-layer anisotropic model with an upper layer close to the strike of the southern segment of the DST that can explain the splitting data. The theoretical curves, the value of model parameters and misfit error for a model with lower layer fast symmetry axis subparallel to the strike of the southern DST are very similar to other selected models presented in Table 1. However, as this lower layer fast axis is fairly uniform over the whole length of the DST from

Table 2. Two-Layer Models Obtained for the Southern DST From the Modeling of the Azimuthal Variations in the Splitting Parameters While the Fast Direction in Either the Upper or Lower Layer is Constrained to Vary Around the Strike of the Fault (Between 16° and 22°)

	Lower Layer		Upper Layer		Misfit Errors		
Sothern DST	Φ (°)	δt (s)	Φ (°)	δt (s)	Φ (°)	δt (s)	Total Variance
Upper layer fast direction fixed	87	0.3	16	1.5	11.1	0.12	2.0500
Lower layer fast direction fixed	22	1.2	−23	0.4	2.3	0.04	0.4934

south to north, it is unlikely that the lower layer is related to the shearing of the faults system itself. This test suggests that neither the upper nor the lower layers aligns with the strike of the southern segment of the DST.

[14] If we assume that the two-layer anisotropy is extended uniformly beneath the Dead Sea region, one may assume that the upper layer represents the anisotropic structure of the lithosphere and the lower layer is related to asthenospheric flow. The thin lithosphere beneath the DST region (less than 80 km [e.g., *Weber et al*., 2009]), however, is unlikely to generate delay times larger than 0.7 s by taking a typical 4% for the bulk upper mantle anisotropy and also assuming coherent deformation over the entire thickness of the lithosphere including the crust. This information may be used to select the most favorable model in each group. The models in each group with delay times in the upper layer not greater than 0.7 s are shown in Table 3. The deeper layer in the final best selected models has fast axis ~25° and delay times ~0.8 s. The fast axis in the upper layer varies between −4° and −13°, and the delay time ranges from 0.60 to 0.7 s. The variations in the upper layer fast axis along the DST may be indicative of crustal contribution to the upper layer anisotropy.

[15] By waveform modeling of splitting data in different frequency ranges along a very dense profile of seismic stations across the southern DST, *Rümpker et al*. [2003] proposed a 2-D anisotropic model for that segment of the DST. As their observations were obtained at relatively short periods from a single event with a spatial sampling of approximately 3 km, we may not test their 2-D model using our data set. Instead, we deduce an average 1-D model from the model proposed by *Rümpker et al*. [2003] consisting of an upper layer with delay time 0.5 s and fast axis −15° and a lower layer with delay time 0.9 s and fast axis 10°. The splitting parameters for the two layers (obtained from the frequency-dependent splitting analysis) are similar to those obtained from the back azimuthal variations presented here. We may take this as an independent support for our analysis.

3.3.2. Cross-Convolution Inversion

[16] Another approach to exploring the depth-dependent anisotropy is modeling the split waveforms rather than the splitting parameters. *Hartog and Schwartz* [2001] showed that the waveforms do not necessarily provide much more constraint on the models than the splitting parameters. However, as the waveforms yield null measurements at some back azimuths, the incorporation of the waveforms provides a more complete azimuthal coverage. We follow the approach of *Menke and Levin* [2003] to calculate the cross-convolution functions from the horizontal split seismograms. A brief description of the approach is given here. In this approach, two horizontal impulse response time series are calculated as functions of the model parameters that when cross-convolved with the observed horizontal split seismograms yield convolution time series that most resemble each other when the model parameters are correctly selected. Following *Menke and Levin* [2003], we compute a penalty function $E(\mathbf{m})$

$$E(\mathbf{m}) = \left(\frac{1}{N}\right)\sum_{i=1}^{N} \|x_i(t) - y_i(t)\|^2 = \left(\frac{1}{N}\right)\sum_{i=1}^{N} \frac{\int [x_i(t) - y_i(t)]^2 dt}{\int x_i^2(t)dt + \int y_i^2(t)dt},$$

where

$$x_i(t) = h_T^{pre}(\mathbf{m}, t) * R_i^{obs}(t) \quad , \quad y_i(t) = h_R^{pre}(\mathbf{m}, t) * T_i^{obs}(t),$$

R_i^{obs} and T_i^{obs} are the radial and tangential components of the

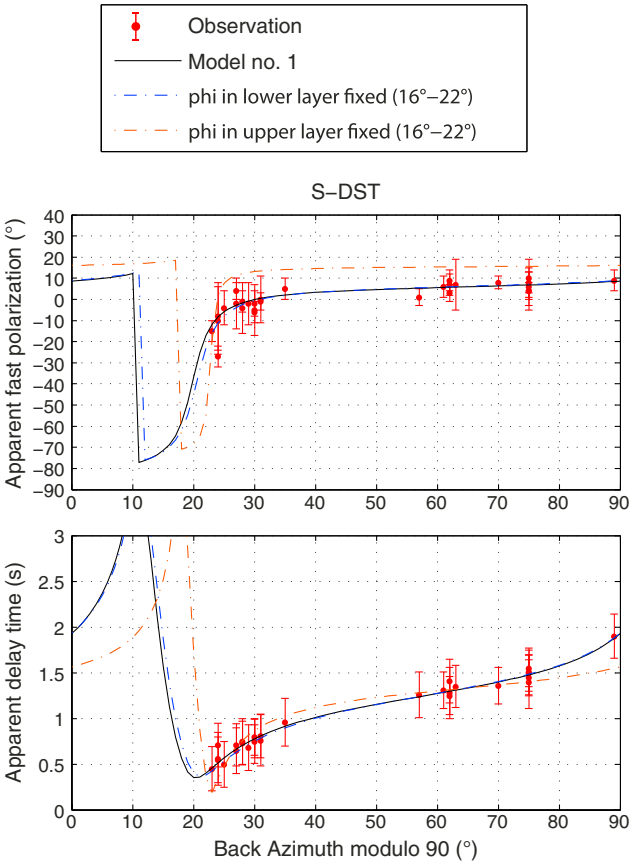

Figure 6. Theoretical predictions of the variations in the apparent splitting parameters with the initial polarization from the two-layer models obtained from the back azimuthal variations of the observed splitting parameters for the southern DST when either the upper or lower layer is confined to vary only around a predetermined value (16°–22°). The model specifications are given in Table 2. The theoretical curve from the best selected model for the southern DST where all four model parameters can freely vary (Figure 5 and Table 3) is also shown for comparison.

Table 3. Final Two-Layer Models Selected for Each Group of Stations Along the DST

Region	Lower Layer		Upper Layer		Misfit Errors		Total Variance
	Φ (°)	δt (s)	Φ (°)	δt (s)	Φ (°)	δt (s)	
Northern DST	25	0.8	−8	0.6	3.3	0.07	0.8868
Central DST	24	0.8	−13	0.6	1.2	0.04	0.3887
Southern DST	26	0.8	−4	0.6	2.4	0.04	0.4926
Whole DST	26	0.7	−6	0.7	4.1	0.14	1.1919

i^{th} waveforms, $h_R^{pre}(\mathbf{m}, t)$ and $h_T^{pre}(\mathbf{m}, t)$ are the radial and tangential impulse responses of the model, and "*" denotes the convolution operator. An optimum model is one having impulse responses that when cross-convolved with the observed horizontal waveforms yield convolution time series $x_i(t)$ and $y_i(t)$, which are the most similar in a sense making the penalty function $E(\boldsymbol{m})$ minimum. The advantage of this approach is that there is no need to estimate an initial wavelet, which is normally required in conventional waveform modeling. We selected those waveforms with high signal-to-noise ratios and simple pulse shapes. We normalize each convolution function by its maximum absolute amplitude to avoid a bias caused by using seismograms with differing amplitudes.

[17] We use a coefficient of determination R^2 as mentioned by *Walker et al.* [2004] to assess the degree to which a two-layer model fits the split waveforms better than a one-layer model

$$R^2 = 1 - \frac{(M-1)}{(M-k-1)}\left(\frac{E_{\min}^{2\ \text{layer}}}{E_{\min}^{1\ \text{layer}}}\right),$$

where $E_{\min}^{2\ \text{layer}}$ and $E_{\min}^{1\ \text{layer}}$ are the values of the penalty functions for the "optimum" two-layer and one-layer models that best fit the convolution functions, respectively. $k = 4$ is the number of the model parameters for a two-layer model.

[18] The number of degrees of freedom of the data is calculated by

$$M = \sum_{i=1}^{N}(K_i B_i),$$

where N is the number of the seismograms used, K_i is the number of samples of each seismogram, and B_i is the bandwidth of each seismogram (ratio of the dominant frequency to the Nyquist frequency). The "dominant frequency" is taken to be 0.1 Hz for SKS waves. For example, for a set of 30 radial components and 30 corresponding tangential components, each sampled with a frequency of 50 samples per seconds (Nyquist frequency 25 Hz), selected over a window length of 15 s (750 samples) and with a fixed dominant frequency of 0.1 Hz, the number of degrees of freedom is 180. The number of degrees of freedom for the same set but with a fixed dominant frequency of 1/8 Hz (dominant period of 8 s) is 225. The coefficient of determination is adjusted by the degree of freedom in order to avoid any bias by using different number of seismograms, sampling rate of the waveforms, and the frequency content of each waveform.

[19] The waveform inversion also suffers from the nonuniqueness inherent in the inversion of split data set. It means that when the grid search seeks four anisotropic parameters of two-layer models, there would be a wide range of model parameter sets that can explain the waveforms within the confidence interval of the waveform fitting penalty function. In order to examine this nonuniqueness, we first search for the best fit models allowing the delay times and fast axes in the upper and lower layers to vary freely (delay times in the range of 0–3 s and fast axes between 0° and 180°). In a second search, we impose the constraint that the delay time in the upper layer does not exceed 0.7 s. The two-layer models obtained from the cross-convolution modeling of the split *KS waveforms for the southern, central, and northern segments of the DST as well as for the whole set of the DESERT and ISN stations are given in Table 4. Table 5 lists the one-layer models obtained for the four groups of stations using cross-convolution inversion. Interestingly, when the four model parameters are let free, the best two-layer models approach a one-layer model, while the two-layer models do not provide a better waveform fitting than one-layer models as illustrated by the respective coefficients of determination (Table 4). On the other hand, when the upper layer delay time is restricted to vary only between 0 and 0.7 s, the best fit models are consistent with those identified earlier by using splitting parameters (Table 3). We therefore postulate that the two-layer models with the delay time in the upper layer less than 0.7 s better explain both the splitting parameters and the split waveforms. The cross-convolution time series from the best fit models for each group of stations are plotted in Figure S2.

3.3.3. Lateral Variations in Splitting Parameters Across the Southern Segment of the DST

[20] The 1-D models inferred from the azimuthal variations of splitting parameters reveal that two layers of anisotropy exist in the proximity of the surface trace of the DST. However, since we do not have splitting observations with a sufficient azimuthal coverage at any of the stations outside of the shear zone, we are not able to conclude that the two-layer models

Table 4. Two-Layer Models Obtained From the Cross-Convolution Modeling of the *KS Waveforms for the Three Groups of Stations and the Whole Set of the DESERT and ISN Stations Along the DST

Region	Lower Layer		Upper Layer		Coefficient of Determination
	Φ (°)	δt (s)	Φ (°)	δt (s)	
Northern DST (four parameters free)	52	0.3	4	1.2	30.6%
Northern DST (with the constraint δt2 ≤ 0.7 s)	25	0.7	−3	0.7	34.0%
Central DST (four parameters free)	52	0.4	−2	1.0	20.4%
Central DST (with the constraint δt2 ≤ 0.7 s)	23	0.7	−14	0.6	27.5%
Southern DST (four parameters free)	30	0.6	−2	0.7	30.3%
Southern DST (with the constraint δt2 ≤ 0.7 s)	26	0.7	−3	0.7	37.2%
Whole DST (four parameters free)	71	0.4	4	1.3	25.0%
Whole DST (with the constraint δt2 ≤ 0.7 s)	25	0.7	−5	0.7	29.0%

Table 5. One-Layer Models Obtained From the Cross-Convolution Modeling of the *KS Waveforms for the Four Groups of Stations Along the DST

Region	Φ (°)	δt (s)
Northern DST	10	1.4
Central DST	5	1.2
Southern DST	10	1.2
Whole DST	9	1.3

extend laterally. We expect that 2-D modeling of observations across the DST can help to constrain the lateral extent of 1-D two-layer models. Figure 7 presents the lateral variations in the observed splitting parameters at stations around the DST southern segment projected onto a profile across the DST (Figure 3a). This includes 42 (non-null) measurements obtained from the back azimuth modulo 90 between 40° and 80°. We selected this limited azimuthal window to avoid the effects of vertical variations in anisotropic structure beneath the individual stations. Φ and δt vary insignificantly with distance away from the fault, the values of δt and Φ being close to 1.3 s and 10°, respectively. As discussed previously, our observations show clear evidence for depth variations of anisotropy at stations close to the DST. However, we cannot exclude such depth variations at more distant stations due to the lack of azimuthal coverage. In the following, we attempt to constrain the width of the two-layer anisotropic zone by 2-D waveform modeling.

3.3.4. Waveform Modeling

[21] In order to explain the observed trend of the splitting parameters across the southern part of the DST, we seek 2-D models of anisotropic structures that can explain the waveforms. We use a 2-D finite difference approach to solve the complete wave equation in an elastic anisotropic medium. A general orthorhombic elastic tensor with a horizontal fast axis is applied throughout the crust and mantle. In the mantle, the fast axis can be interpreted as the a-axis of olivine. For the crust, we interpret the fast axis as the symmetry axis of a medium with vertical aligned fractures. The 2-D models consist of blocks that are defined by the isotropic reference velocities of *P* and *S* waves, percentage of anisotropy, fast symmetry axis direction, and density. The coordinate axes in our 2-D models are chosen such that the properties of each block change vertically with depth (z-direction) and horizontally in direction perpendicular to the trend of the fault (*x* axis). Receiver function analysis [*Hofstetter and Bock*, 2004; *Mohsen et al.*, 2005; *Weber et al.*, 2009; *Mohsen et al.*, 2011] and active seismic surveys [*Hofstetter et al.*, 1991, 2000; *Mechie et al.*, 2005; *Weber et al.*, 2009; *Mechie et al.*, 2009] indicate that the crustal thickness increases smoothly across the southern DST from ~28 km in the west to ~35 km in the east without any abrupt jump in the Moho beneath the surface trace of the DST. Our modeling showed that such a gradual change in the crustal thickness has no significant effect on the lateral variations in the observed splitting parameters. We therefore assume a flat Moho interface in our models. For each model, a bottom isotropic layer is assumed from where the initial wavefront begins propagating vertically upward into the upper layers of the model to reach on the surface. As no approximation is assumed to solve the wave equation, in addition to splitting in the anisotropic medium, many other wave phenomena such as diffraction, scattering, and wavefront healing are also observable in the synthetic seismograms. The wavefield is recorded on the surface by a linear array of detectors. The computed synthetic seismograms using initial wavelets with different initial polarization directions are then treated by the same procedure that is used for the observed data set. The splitting parameters obtained from the synthetic seismograms are then compared the observed parameters from the real data. As the initial wavelets may be different from those of the real data, the synthetic and real waveforms are not directly compared.

3.3.4.1. Model 1

[22] As the splitting parameters change only slightly across the fault (Figure 7), a first model that can explain the observations is one with laterally uniform properties. As a simplest candidate model, a one-layer anisotropic model without any lateral variations in elastic properties can produce splitting parameters that do not exhibit lateral and azimuthal variations. However, as described previously, our observations of splitting parameters at stations near the trace of the fault exhibit clear azimuthal variations that are indicative of a depth-dependent anisotropy. The 1-D models obtained for these stations consist of two anisotropic layers with an upper layer of near N-S (−4°) fast direction and a lower layer of NE-SW (26°) fast direction. The delay time in the upper layer is 0.6–0.7 s and in the lower layer is 0.7–0.8 s.

[23] Petrophysical evidence [e.g., *Mainprice et al.*, 2005] suggests that dislocation creep leading to the preferred orientation of mantle minerals takes place in the uppermost 300 km of the mantle. This means that the main source of the SKS splitting signals resides in the lithosphere and/or the underlying asthenosphere. By taking the typical values of 4% to 5% for the magnitude of anisotropy of mantle rocks [e.g., *Ben Ismail and Mainprice*, 1998; *Mainprice*, 2000], delay times of 0.6–0.7 s for the upper anisotropic layer in our 1-D models require a 50–80 km thick anisotropic layer. Considering that the lithosphere beneath the DST region is

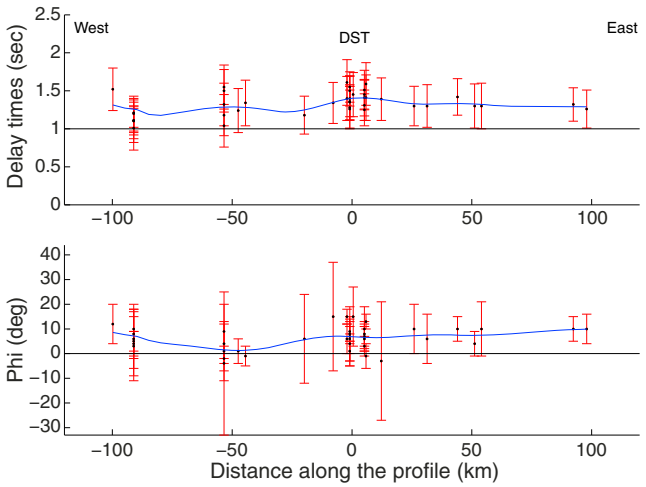

Figure 7. Profile of splitting parameters observed across the southern segment of the DST from events occurred at back azimuths (modulo 90) between 40° and 80°. The distances along the profile are relative to the position of the trace of the DST on the surface. The blue line is a smoothed curve passed through the observed points representing the general trend of the variations along the profile.

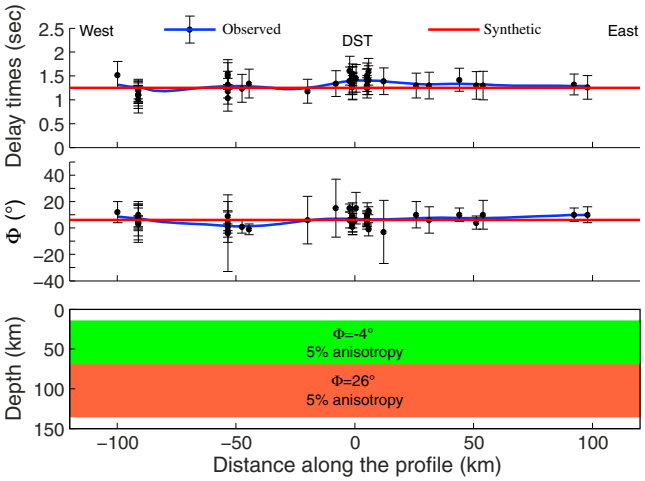

Figure 8. (bottom) A model consisting of two anisotropic layers without any lateral variations across the DST. (middle) Apparent fast polarization direction obtained from the synthetic waveforms (red curve) and observed apparent fast polarization direction (black dots with error bars and blue average curve). (top) Apparent split delay times produced from this model (red curve) and observed delay times (black dots with error bars and blue average curve). The blue line is a smoothed curve passed through the observed points.

only ~70 km thick [*Mohsen et al*., 2006; *Laske et al*., 2008; *Weber et al*., 2009], including a 30–35 km thick crust, some contribution from the crust and/or sublithospheric asthenosphere is also required to produce the proposed delay time in the upper layer. The deeper layer represents a ~80 km thick anisotropic layer assuming 4% anisotropy.

[24] In this first model, we therefore assume the two-layer anisotropy extends on both sides of the DST beneath the Sinai subplate and Arabian Plate. For the purpose of modeling, we assume that the upper layer depth extension is from 15 km down to 70 km assuming a vertically coherent deformation between the lower crust and mantle lithosphere. The deeper layer, extending from 70 km to 135 km depth, is thought to be related to an asthenospheric flow field. Figure 8 shows a model consisting of a 55 km thick upper layer with a fast axis of −4° and 5% anisotropy overlying a 65 km lower layer with a fast axis of 26 and 5% anisotropy according to the 1-D models obtained for the southern DST (Tables 3 and 4). The splitting analysis of the synthetic waveforms from such a laterally uniform two-layer model produces laterally invariant apparent splitting parameters that fit our observation, except for some minor variations. In principle, the two anisotropic layers can be shifted vertically to yield the same pattern of splitting parameters at the surface. One possibility, not explicitly shown here, is that both layers reside in the mantle without a partial crustal contribution. In such a case, the upper layer may represent the mantle lithosphere together with the uppermost part of the asthenosphere assuming a coherent deformation. The lower layer would then correspond to the deeper part of the asthenosphere.

3.3.4.2. Model 2

[25] While our observations for stations close to the fault favor a two-layer model, the observations for stations at greater distance to the fault do not allow discriminating between a one and multilayer model. One may therefore assume a vertically uniform anisotropic layer at greater distances from the fault. Such a model has also been proposed for the San Andreas fault system [e.g., *Ozalaybey and Savage*, 1995; *Hartog and Schwartz*, 2001; *Polet and Kanamori*, 2002; *Bonnin et al*., 2010], where an asthenospheric layer is assumed to extend regionally beneath and outside the faults zone whereas shear-zone-related anisotropy in the lithosphere is confined to the immediate vicinity of the fault system. In model 2 (Figure 9), we therefore assume that a vertically coherent anisotropic fabric is developed in the fault shear zone from the surface to the base of the lithosphere at a depth of 70 km. The fault shear zone is assumed to widen with depth from 20 km at the surface to 40 km at a depth of 70 km. The fast direction in this lithospheric layer is taken at −4° and the strength of anisotropy at 4% according to the two-layer models shown in Tables 3 and 4. A lower layer with a fast symmetry direction of 26° is supposed to extend beneath the whole width of the model for the depth ranges 70–150 km with 4% of anisotropy. However, this model yields laterally varying splitting parameters that do not match the observed slightly varying trend (Figure 9).

3.3.4.3. Model 3

[26] We now assume that both the central zone of two anisotropic layers and the outside region of one anisotropic layer extend from the surface across the lithosphere into the asthenosphere (Figure 10). This model generates apparent splitting parameters that better fit the observations, and there is some similarity to previously discussed models of anisotropy in the vicinity of the DST [*Rümpker et al*., 2003]. However, one cannot easily justify the development of a vertically coherent fabric from the surface down into the asthenosphere in the region outside the transform fault,

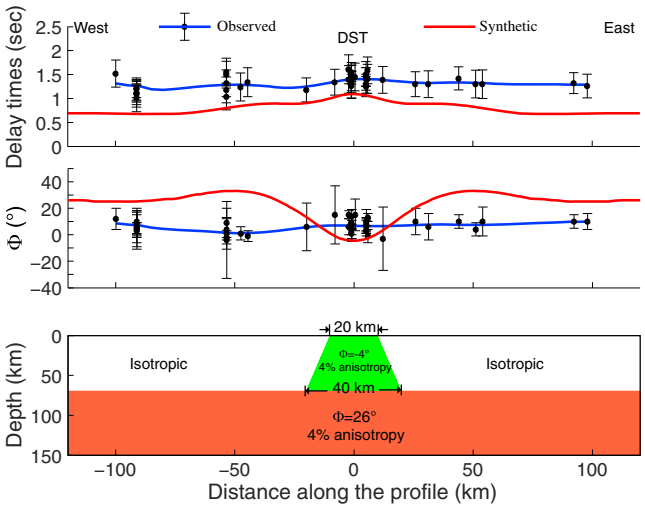

Figure 9. (bottom) A model consisting of a central block of two anisotropic layers extending from the surface up to a depth of 70 km that widens from 20 km at the surface to 40 km at the depth of 70 km and one-layer side blocks extending from 70 km to 150 km depth. (middle) Apparent fast polarization direction obtained from the synthetic waveforms from model and observed apparent fast polarization direction. (top) Apparent split delay times produced from this model and observed delay times.

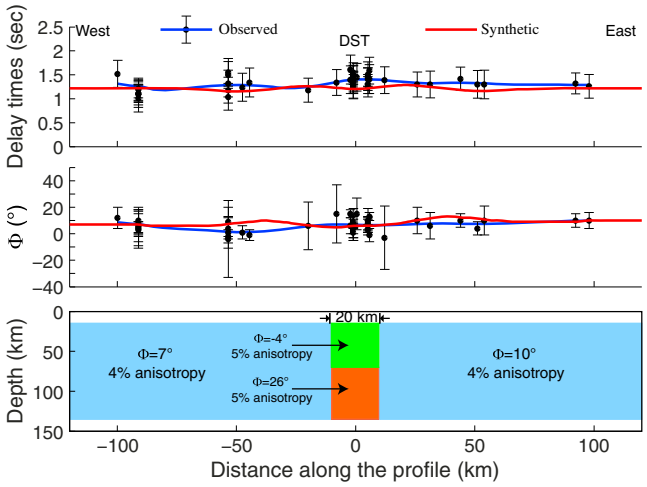

Figure 10. (bottom) A model consisting of a 20 km wide central block of two anisotropic layers extending from the surface up to a depth of 140 km and one-layer side blocks extending from the surface to a depth of 140 km. (middle) Apparent fast polarization direction obtained from the synthetic waveforms from model and observed apparent fast polarization direction. (top) Apparent split delay times produced from this model and observed delay times.

whereas such fabric may be expected within the immediate vicinity of the fault. However, although the fast direction in the lower layer (26°) is close to the strike of the southern segment of the DST, the fast direction in the upper layer (−4°) does not agree with the strike-slip shearing. It is therefore difficult to explain the presence of the two-layer central zone and only one layer outside of it.

[27] One may seek more models with laterally varying anisotropic structures residing at different depths. Substantial lateral heterogeneity in elastic properties may cause the apparent splitting parameters to vary across the DST. As pointed out previously by *Rümpker and Ryberg* [2000] and *Kaviani et al*. [2011], lateral variations in isotropic and/or anisotropic structures in the crust do have effects on the apparent splitting parameter at distances away from the boundaries of the lateral changes. The extremely dense station spacing (of less than 3 km) in the studies of *Rümpker et al*. [2003] and *Ryberg et al*. [2005] prevents a direct comparison with observations presented here. This may be the reason, that, in our waveform modeling (and larger station spacing), there is no need for a narrow zone of fault-related olivine alignment.

[28] We further note that we assume a vertically propagating wavefront. Lateral variations in elastic properties may have notable effects on the wave propagation when nonvertical paths are considered. However, at this point, to consider more complex models of anisotropy and heterogeneity is difficult to justify in view of the observational results.

4. Discussion

[29] This study provides the first detailed investigation of polarization seismic anisotropy along the DST using dense networks of stations. The results of our shear wave splitting analysis are generally in agreement with the previous studies carried out in the region. *Schmid et al*. [2004] reported coherent mean N-S fast directions and delay times around 1.4 s at three permanent stations EIL, JER, and MRNI that are also used in our study. They relate their average splitting parameters to the mantle anisotropy in the shear zone along the DST due to the differential motion between Arabia and Africa. *Levin et al*. [2006] analyzed SKS waveforms recorded at permanent stations EIL, JER, KSDI, and MRNI along the trace of the DST and at a single temporary station HIT located in the Arabian plate east of the southern segment of the DST. They used the cross-convolution method to infer one or two-layer models beneath the trace of the DST. Their one-layer models are in agreement with our one layer models with fast directions 12°–19° and average delay time of ~1.3 s. Their two-layer models at stations JER, EIL, and HIT are consistent with each other and consist of an upper layer with fast directions striking NNE and delay times between 1.1–1.7 s. The lower layer beneath these stations has fast axis varying between 50° and 80° with delay times of 0.5–1.0 s. For the combination of the northern stations KSDI and MRNI, *Levin et al*. [2006] suggest a two-layer model consisting of an upper layer with an N-S fast axis direction and a delay time of ~1.0 s and a lower layer with a fast axis of ~30° and a delay time of ~1.0 s. The fast symmetry directions in our models at four groups of stations along the DST are more consistent with the model proposed by *Levin et al*. [2006] for the northern stations. The delay times in our models are, however, lower than those found by *Levin et al*. [2006]. The fast symmetry axes in the upper and lower layers of the model proposed by *Levin et al*. [2006] are consistent with those in our models. However, the delay times attributed to each layer by *Levin et al*. [2006] are higher than those obtained in our models. We postulate that the higher delay time in their upper layer is difficult to explain by the relatively thin lithosphere beneath the region. *Levin et al*. [2006] attribute the anisotropy in the lower layer to the relative motion between the lithospheric plates and the underlying asthenosphere. They leave open the question of whether the source of anisotropy in the upper layer is due to the shearing along the DST or is related to a regional anisotropy in the lithosphere of the Arabian plate. They suggest, however, that the impact of the DST on the mantle fabric is probably weak. Our findings provide new constraints in support of the hypothesis that the contribution of the shearing along the DST to the development of the mantle fabric is weak. Alternatively, however, the shear zone may be too narrow to be detectable by our measurements. The waveform modeling of *Rümpker et al*. [2003] and *Ryberg et al*. [2005] suggests the presence of a narrow ~20 km wide subcrustal vertical anisotropic zone beneath the DST that extends through the entire lithosphere. Thermodynamic modeling [*Sobolev et al*., 2005] also suggests the presence of a 20–30 km wide shear zone beneath the surface trace of the DST that cuts through the entire lithosphere. On the other hand, the relatively narrow vertical corridor of possibly low-velocity zone around the trace of the DST could not be resolved by the teleseismic imaging of *Koulakov et al*. [2006]. Our 1-D models obtained from the azimuthal variations in apparent splitting parameters as well as from cross-convolution functions of the split horizontal component waveforms suggest two-layer models for the stations along the trace of the DST that are similar to those presented by *Rümpker et al*. [2003] and *Ryberg et al*. [2005] for areas close to the trace of the DST. However, our 2-D models across the southern trace of the DST suggest that the two-layer model is not restricted to the proximity of the

surface trace of the DST but rather extends over a region away from the fault zone. The modeling determined that even if the shear zone associated with the faults system widens with depth, the related anisotropic model cannot generate the observed features of the splitting at the surface. This evidence implies that the DST itself does not widely contribute to the development of the anisotropic structures at depth. Here we argue that the two-layer model represents one anisotropic layer in the mantle lithosphere and one deeper asthenospheric layer.

[30] Seismological studies [*Hofstetter and Bock*, 2004; *Mohsen et al*., 2006; *Laske et al*., 2008; *Weber et al*., 2009] suggest a relatively fast but thin lithosphere beneath the DST. These studies showed that the mantle lid in the western side of the DST is about 80 km thick, and in the eastern side, it is no thicker than 65 km. *Petrunin et al*. [2012] propose that the lithosphere beneath the DST was thinned and weakened by thermal erosion of the base of the lithosphere as a result of the interaction with a thermo-chemical mantle plume occurred about 20 Ma, which began before and continued during the active faulting along the DST. Unless an exceptionally high degree of anisotropy is assumed for the thinned mantle lithosphere (~35 km) beneath the Dead Sea region, then a contribution from the overlying crust and/or underlying asthenosphere is needed to explain the delay time of the upper anisotropic layer in our models. Coherent deformation between the mechanically weakened mantle lithosphere and the underlying asthenosphere can create an anisotropic layer thick enough to simulate the delay time in the upper layer of our models.

[31] As the DST cuts through a continental lithosphere that has not undergone any significant deformation regime since the Cambrian and before inception of the strike-slip motion along the DST itself, the likely pervasive fabrics in the lithosphere on both sides of the DST are expected to be those created and preserved from the Precambrian Pan-African Orogeny. On the other hand, the relatively recent basal heating/erosion [~20 Ma, *Petrunin et al*., 2012] could have reworked any older anisotropic fabric in the mantle lithosphere on both sides of the DST. Farther east on the Arabian shield and platform, *Hansen et al*. [2006] did not observe any correlation between the changes in the lithosphere thickness and the lateral variations in their shear wave splitting observations. They attributed their observed splitting parameters to the anisotropy in the asthenosphere resulting from a combination of a flow in the absolute plate motion direction and a channelized flow along the Red Sea originated from the Afar upwelling. They did not, however, examine the possibility of two-layer anisotropy beneath the Arabian Shield and Platform. Farther north in the Turkish-Anatolian plateau, *Sandvol et al*. [2003] and *Biryol et al*. [2010] observed that shear wave splitting parameters do not change across the major plate boundaries. This fact led these authors to suggest that uniform mantle anisotropy exists across the major plate boundaries favoring an asthenospheric anisotropy over a lithospheric source. Their short-term observation, however, did not allow for precise modeling of azimuthal variations of splitting parameters for multilayer anisotropy. Our modeling shows that the two-layer model found for the Dead Sea region may extend to the surrounding regions. Further detailed analysis of splitting data at permanent stations in the Middle East is required to examine this hypothesis.

[32] Recent GPS survey around the DST [*al Tarazi et al*., 2011] showed that the lithospheric plates move in the NE direction in the ITRF2005 no-net-rotation reference frame. If we assume this to represent the relative motion between the lithosphere and the underlying asthenosphere, a flow in the asthenosphere occurs subparallel to this motion. If it is true, we expect one bottom layer of anisotropy in the NE direction, which is uniformly distributed in the region. On the other hand, a recent investigation of the deep 3-D S-velocity structure beneath Arabia and East Africa [*Chang and Van der Lee*, 2011] by joint inversion of multiple geophysical data set mapped out the occurrence of a quasi-vertical low-velocity anomaly beneath Jordan and northern Arabia that, they believe, can be a mantle plume responsible for the widespread Neogene volcanism in the region. These authors argue against the general notion of the channeled flow of the Afar upwelling materials along the Red Sea. Instead they propose that the upwelled materials in the Afar are rather channeled northward beneath Arabia. If this idea is correct, our shear wave splitting observations around the DST would not be affected by the Afar plume. On the other hand, *Chang and Van der Lee* [2011] suggest that the Jordan plume materials can be channelized horizontally along the DST. This implies that the deeper anisotropic layer in our models may have been affected by the horizontal flow due to this possible plume beneath the region.

4.1. Comparison With San Andreas Fault

[33] Shear wave splitting studies in the region of the SAF system in southern California showed that at stations in the vicinity of the surface trace of the fault system, the splitting parameters exhibit significant variations with back azimuth [e.g., *Ozalaybey and Savage*, 1995; *Hartog and Schwartz*, 2001; *Polet and Kanamori*, 2002; *Bonnin et al*., 2010]. These azimuthal variations can be accounted for by two-layer anisotropic models with an upper layer of fault-parallel fast direction overlying a deeper layer with an E-W fast direction. The upper layer is characterized by a delay time of ~0.7 s, and the lower layer is characterized by a twice larger delay time of ~1.5 s. The upper layer is interpreted to be in the lithosphere and is related to the finite strain along the faults system associated with the differential motion between the North American and Pacific plate. The deeper layer has the same characteristics as the regional anisotropy and is thought to be created by flow in the asthenosphere due to either the motion of the lithospheric plates over the asthenosphere [*Hartog and Schwartz*, 2001; *Bonnin et al*., 2010] or the local flows in the asthenosphere generated in the slabless window left behind the Farallon plate [*Ozalaybey and Savage*, 1995]. Recently, by performing a forward modeling of deformation and wave propagation, *Bonnin et al*. [2012] showed that SKS splitting observations in Central California are best fitted by a model with a hotter geotherm beneath the North American plate within 60 km of the plate boundary, representing an asthenosphere window related to the northward migration of the Mendocino Triple Junction. Their modeling furthermore revealed that the westward migration of the plate boundary cannot explain the rotation of the fast polarization directions. The model of deformation and development of fabric in the mantle by *Bonnin et al*. [2012] shows that the shearing along the plate boundary plays the major role in development of mantle anisotropy beneath the plate

boundary. Their modeling also reveals that the mantle anisotropic fabric beneath the Pacific and North American plates is developed by differential motions of lithospheric plates over the underlying mantle but is strongly dependent upon the preexisting fabric in the mantle. This modeling unveiled that the present-day fabric beneath the lithosphere plates outside the plate boundaries may be strongly inherited from preexisting fabrics.

[34] Our observations and 1-D models show that in the case of the DST, unlike the two-layer model beneath the SAF, the two anisotropic layers have nearly the same delay times, between 0.5 and 0.8 s. Furthermore, our 2-D finite difference modeling of the split waveforms observed across the southern DST shows that, unlike the SAF, a model with an anisotropic layer in the lithosphere laterally confined around the trace of the DST overlying a regionally extended asthenospheric layer does not favor the observations.

[35] The SAF, with higher slip rate (30–50 mm/yr, [e.g., *DeMets and Dixon*, 1999; *Bennett et al*., 1996]) and older age (Oligocene, [e.g., *Atwater*, 1970]), has accommodated more than 500 km [e.g., *van der Woerd et al*., 2006] of relative motion between the Pacific and North American plates. This indicates that the SAF had enough time to generate pervasive fabric along the shear zone. However, the DST, with a comparatively slow slip rate (4–5 mm/yr, [*al Tarazi et al*., 2011; *Mahmoud et al*., 2005]) and younger age (Middle Miocene) did not have enough time to develop a pervasive fabric over the entire thickness of lithosphere.

5. Conclusion

[36] Shear wave splitting observations from dense seismic networks of the DESIRE and DESERT projects and the permanent stations of the Israel Seismic Network provide evidence for two-layer anisotropic models beneath the DST fault. Different two-layer models from 1-D modeling of the azimuthal variations in splitting parameters exhibit very similar properties along the strike of the DST and consist of an upper layer with a nearly N-S oriented fast symmetry axis and a lower layer with an NE-SW fast symmetry axis. The delay times in the upper and lower layer of each model vary between 0.6 and 0.8 s and are almost equally partitioned between the two layers. Further 2-D modeling suggested that the two-layer models may extend beyond the immediate vicinity of the DST. We cannot resolve a distinct contribution of the shearing associated with the DST to the development of the anisotropic fabric beneath the Dead Sea region. We argue that the two anisotropic layers reside in the lithosphere and asthenosphere, respectively. However, further investigations of depth-dependent anisotropy, using for example converted seismic phases, may help to clarify this issue. We also suggest further detailed investigation of azimuthal variations of splitting parameters at permanent stations in the Middle East to examine the variation of depth-dependent anisotropy beneath the region.

[37] **Acknowledgments.** We thank the Geophysical Instrument Pool Potsdam (GIPP) for providing the instruments for the DESERT and DESIRE experiments. GEOFON is also thanked for data archiving. We acknowledge help and support from all the people involved in installation and visit of the seismological stations of both DESERT and DESIRE projects. We further thank the Israel Seismic Network for providing the data from the permanent stations. We are grateful to Vadim Levin and the anonymous reviewer for the very thoughtful and constructive comments and suggestions for improvement of the manuscript. AK has benefited from a research grant by the German Research Foundation (DFG). The maps shown in the paper were created using the GMT software [*Wessel and Smith*, 1991].

References

Atwater, T. (1970), Implications of plate tectonics for the Cenozoic tectonic evolution of western North America, *Geol. Soc. Am. Bull.*, *81*, 3513–3536.

Bartov, Y., G. Steinitz, M. Eyal, and Y. Eyal (1980), Sinistral movement along the Gulf of Aqaba—Its age and relation to the opening of the Red Sea, *Nature*, *285*(5762), 220–222, doi:10.1038/285220a0.

Ben Ismail, W., and D. Mainprice (1998), An olivine fabric database: An overview of upper mantle fabrics and seismic anisotropy, *Tectonophysics*, *296*, 145–157, doi:10.1016/S0040-1951(98)00141-3.

Ben-Avraham, Z., Z. Garfunkel, and M. Lazar (2008), Geology and Evolution of the Southern Dead Sea Transform fault with Emphasis on Subsurface Structure, *Annu. Rev. Earth Planet. Sci.*, *36*, 357–387, doi:10.1146/annurev.earth.36.031207.124201.

Ben-Menahem, A., A. Nur, and M. Vered (1976), Tectonics, seismicity and structure of the Afro-Eurasian junction- the breaking of an incoherent plate, *Phys. Earth Planet. Inter.*, *12*, 1–50.

Bennett, R. A., W. Rodi, and R. E. Reilinger (1996), Global Positioning System constraints on fault slip rates in southern California and northern Baja, Mexico, *J. Geophys. Res.*, *101*, 21,943–21,960.

Biryol, C. B., G. Zandt, S. L. Beck, A. A. Ozacar, H. E. Adiyaman, and C. R. Gans (2010), Shear wave splitting along a nascent plate boundary: The North Anatolian Fault Zone, *Geophys. J. Int.*, *181*, 1201–1213, doi:10.1111/j.1365-246X.2010.04576.x.

Bonnin, M., G. Barruol, and G. H. R. Bokelmann (2010), Upper mantle deformation beneath the North American–Pacific plate boundary in California from SKS splitting, *J. Geophys. Res.*, *115*, B04306, doi:10.1029/2009JB006438.

Bonnin, M., A. Tommasi, R. Hassani, S. Chevrot, J. Wookey, and G. Barruol (2012), Numerical modelling of the upper-mantle anisotropy beneath a migrating strike-slip plate boundary: The San Andreas Fault system, *Geophys. J. Int.*, *191*(2), 436–458.

Bowman, J. R., and M. Ando (1987), Shear-wave splitting in the upper-mantle wedge above the Tonga subduction zone, *Geophys. J. R. Astron. Soc.*, *88*, 25–41.

Chang, S.-J., and S. Van der Lee (2011), Mantle plumes and associated flow beneath Arabia and East Africa, *Earth Planet. Sci. Lett.*, *302*(3–4), 448–454, doi:10.1016/j.epsl.2010.12.050.

Crampin, S. (1978), Seismic wave propagation through a cracked solid: Polarization as a possible dilatancy diagnostic, *Geophys. J. R. Astron. Soc.*, *53*, 467–496.

Crampin, S. (1987), Geological and industrial implications of extensive-dilatancy anisotropy, *Nature*, *328*, 491–496.

DeMets, C., and T. H. Dixon (1999), New kinematic models for Pacific–North America motion from 3 Ma to present, I: Evidence for steady motion and biases in the NUVEL-1A model, *Geophys. Res. Lett.*, *26*, 1921–1924.

Freund, R., Z. Garfunkel, I. Zak, M. Goldberg, T. Weissbrod, and B. Derin (1970), The shear along the Dead Sea rift, *Philos. Trans. R. Soc. London, Ser. A*, *267*, 107–130.

Garfunkel, Z. (1981), Internal structure of the Dead Sea leaky transform (rift) in relation to plate kinematics, *Tectonophysics*, *80*(1–4), 81–108, doi:10.1016/0040-1951(81)90143-8.

Garfunkel, Z., and Z. Ben-Avraham (1996), The structure of the Dead Sea basin, *Tectonophysics*, *266*(1–4), 155–176, doi:10.1016/S0040-1951(96)00188-6.

Hansen, S., S. Schwartz, A. Al-Amri, and A. Rodgers (2006), Combined plate motion and density-driven flow in the asthenosphere beneath Saudi Arabia: Evidence from shear-wave splitting and seismic anisotropy, *Geology*, *34*(10), 869–872, doi:10.1130/G22713.1.

Hartog, R., and S. Schwartz (2001), Depth dependent mantle anisotropy below the San Andreas Fault system: Apparent splitting parameters and waveforms, *J. Geophys. Res.*, *106*, 4155–4167, doi:10.1029/2000JB900382.

Hofstetter, A., and G. Bock (2004), Shear-wave velocity structure of the Sinai sub-plate from receiver function analysis, *Geophys. J. Int.*, *158*, 67–84.

Hofstetter, A., L. Feldman, and Y. Rotstein (1991), Crustal structure of Israel: constraints from teleseismic and gravity data, *Geophys. J. Int.*, *104*, 371–379.

Hofstetter, A., C. Dorbath, M. Rybakov, and V. Goldshmidt (2000), Crustal and upper mantle structure across the Dead Sea rift and Israel from teleseismic P wave tomography and gravity data, *Tectonophysics*, *327*, 37–59.

Kaviani, A., G. Rümpker, M. Weber, and G. Asch (2011), Short-scale variations of shear-wave splitting across the Dead Sea basin: Evidence for the

effects of sedimentary fill, *Geophys. Res. Lett.*, *38*, L04308, doi:10.1029/2010GL046464.

Koulakov, I., S. V. Sobolev, M. Weber, S. Oreshin, K. Wylegalla, and R. Hofstetter (2006), Teleseismic tomography reveals no signature of the Dead Sea Transform in the upper mantle structure, Earth Planet, *Sci. Lett.*, *252*, 189–200, doi:10.1016/j.epsl.2006.09.039.

Laske, G., M. Weber, and the DESERT Working Group (2008), Lithosphere structure across the Dead Sea Transform as constrained by Rayleigh waves observed during the DESERT experiment, *Geophys. J. Int.*, *173*, 593–610, doi:10.1111/j.1365-246X.2008.03749.x.

Le Beon, M., Y. Klinger, A.-Q. Amrat, A. Agnon, L. Dorbath, G. Baer, J.-C. Ruegg, O. Charade, and O. Mayyas (2008), Slip rate and locking depth from GPS profiles across the southern Dead Sea Transform, *J. Geophys. Res.*, *113*, B11403, doi:10.1029/2007JB005280.

Leary, P. C., S. Crampin, and T. V. McEvilly (1990), Seismic fracture anisotropy in the Earth's crust: An overview, *J. Geophys. Res*., *95*, 11,105–11,114.

Levin, V., A. Henza, J. Park, and A. Rodgers (2006), Texture of mantle lithosphere along the Dead Sea Rift: recently imposed or inherited?, *Phys. Earth Planet. Inter.*, *158*, 174–189.

Long, M. D., and P. G. Silver (2009), Shear wave splitting and mantle anisotropy: measurements, interpretations, and new directions, *Surv. Geophys.*, *30*, 407–461.

Mahmoud, S., R. Reilinger, S. McClusky, P. Vernant, and A. Tealeb (2005), GPS evidence for northward motion of the Sinai block: Implications for E. Mediterranean tectonics, *Earth Planet. Sci. Lett.*, *238*, 217–224.

Mainprice, D. (2000), The estimation of seismic properties of rocks with heterogeneous microstructures using a local cluster model—Preliminary results, *Phys. Chem. Earth*, *25*, 155–161, doi:10.1016/S1464-1895(00)00025–9.

Mainprice, D., A. Tommasi, H. Couvy, and P. Cordier (2005), Pressure sensitivity of olivine slip systems and seismic anisotropy of Earth's upper mantle, *Nature*, *433*, 731–733, doi:10.1038/nature03266.

Mechie, J., K. Abu-Ayyash, Z. Ben-Avraham, R. El-Kelani, A. Mohsen, G. Rümpker, J. Saul, and M. Weber (2005), Crustal shear velocity structure across the Dead Sea Transform from two-dimensional modelling of DESERT project explosion seismic data, *Geophys. J. Int.*, *160*, 910–924, doi:10.1111/j.1365-246X.2005.02526.x.

Mechie, J., K. Abu-Ayyash, Z. Ben-Avraham, R. El-Kelani, I. Qabbani, M. Weber, and DESIRE Group (2009), Crustal structure of the southern Dead Sea basin derived from project DESIRE wide-angle seismic data, *Geophys. J. Int.*, *178*, 457–478, http://dx.doi.org/10.1111/j.1365-246X.2009.04161.x.

Menke, W., and V. Levin (2003), A cross-convolution method for interpreting SKS splitting observations, with application to one and two layer anisotropic earth models, *Geophys. J. Int.*, *154*, 379–392.

Mohsen, A., R. Hofstetter, G. Bock, R. Kind, M. Weber, K. Wylegalla, G. Rümpker, and the DESERT Group (2005), A receiver function study across the Dead Sea Transform, *Geophys. J. Int.*, *160*, 948–960, doi:10.1111/j.1365-246X.2005.02534.x.

Mohsen, A., R. Kind, S. V. Sobolev, and M. Weber (2006), Thickness of the lithosphere east of the Dead Sea Transform, *Geophys. J. Int.*, *167*(2), 845–852, doi:10.1111/j.1365-246X.2006.03185.x.

Mohsen, A., G. Asch, J. Mechie, R. Kind, R. Hofstetter, M. Weber, M. Stiller, and K. Abu- Ayyash (2011), Crustal structure of the Dead Sea Basin (DSB) from a receiver function analysis, *Geophys. J. Int.*, *184*, 463–476, http://dx.doi.org/10.1111/j.1365-246X.2010.04853.x.

Ozalaybey, S., and M. K. Savage (1995), Shear wave splitting beneath the western United States in relation to plate tectonics, *J. Geophys. Res.*, *100*, 18,135–18,149, doi:10.1029/95JB00715.

Petrunin, A. G., E. Meneses Rioseco, S. V. Sobolev, and M. Weber (2012), Thermomechanical model reconciles contradictory geophysical observations at the Dead Sea Basin, *Geochem. Geophys. Geosyst.*, *13*, Q04011, doi:10.1029/2011GC003929.

Polet, J., and H. Kanamori (2002), Anisotropy beneath California: Shear wave splitting measurements using a dense broadband array, *Geophys. J. Int.*, *149*, 313–327, doi:10.1046/j.1365-246X.2002.01630.x.

Quennell, A. M. (1958), The structural and geomorphic evolution of the Dead Sea rift, *Q. J. Geol. Soc.*, *114*, 1–24, doi:10.1144/gsjgs.114.1.0001.

Rümpker, G., and T. Ryberg (2000), New "Fresnel-zone" estimates for shear-wave splitting observations from finite-difference modeling, *Geophys. Res. Lett.*, *27*, 2005–2008.

Rümpker, G., and P. G. Silver (1998), Apparent shear-wave splitting parameters in the presence of vertically varying anisotropy, *Geophys. J. Int.*, *135*, 790–800.

Rümpker, G., T. Ryberg, G. Bock, and Desert Seismology Group (2003), Boundary-layer mantle flow under the Dead Sea Transform fault inferred from seismic anisotropy, *Nature*, *425*, 497–501, doi:10.1038/nature01982.

Ryberg, T., G. Rümpker, C. Haberland, D. Stromeyer, and M. Weber (2005), Simultaneous inversion of shear wave splitting observations from seismic arrays, *J. Geophys. Res.*, *110*, B03301, doi:10.1029/2004JB003303.

Sadeh, M., Y. Hamiel, A. Ziv, Y. Bock, P. Fang, and S. Wdowinski (2012), Crustal deformation along the Dead Sea Transform and the Carmel Fault inferred from 12 years of GPS measurements, *J. Geophys. Res.*, *117*, B08410, doi:10.1029/2012JB009241.

Sandvol, E., N. Turkelli, E. Zor, R. Gok, T. Bekler, C. Gurbuz, D. Seber, and M. Barazangi (2003), Shear wave splitting in a young continent-continent collision: An example from Eastern Turkey, *Geophys. Res. Lett.*, *30*(24), 8041, doi:10.1029/2003GL017390.

Savage, M. K. (1999), Seismic anisotropy and mantle deformation: What have we learned from shear wave splitting?, *Rev. Geophys.*, *37*, 65–106, doi:10.1029/98RG02075.

Schmid, C., S. van der Lee, and D. Giardini (2004), Delay times and shear wave splitting in the Mediterranean region, *Geophys. J. Int.*, *159*, 275–290.

Silver, P. G. (1996), Seismic anisotropy beneath the continents: Probing the depths of Geology, *Annu. Rev. Earth Planet. Sci.*, *24*, 385–432.

Silver, P. G., and W. W. Chan (1991), Shear-wave splitting and subcontinental mantle deformation, *J. Geophys. Res.*, *96*, 16,429–16,454.

Silver, P. G., and M. K. Savage (1994), The interpretation of shear-wave splitting parameters in the presence of two anisotropic layers, *Geophys. J. Int.*, *119*, 949–963.

Sobolev, S. V., A. Petrunin, Z. Garfunkel, A. Y. Babeyko, and the DESERT Group (2005), Thermo-mechanical model of the Dead Sea Transform, Earth Planet. *Sci. Lett.*, *238*, 78–95, doi:10.1016/j.epsl.2005.06.058.

al Tarazi, E., J. Abu Rajab, F. Gomez, W. Cochran, R. Jaafar, and M. Ferry (2011), GPS measurements of near-field deformation along the southern Dead Sea Transform fault System, *Geochem. Geophys. Geosyst.*, *12*, Q12021, doi:10.1029/2011GC003736.

ten Brink, U. S., A. S. Al-Zoubi, C. H. Flores, Y. Rotstein, I. Qabbani, S. H. Harder, and G. R. Keller (2006), Seismic imaging of deep low-velocity zone beneath the Dead Sea basin and transform fault: Implications for strain localization and crustal rigidity, *Geophys. Res. Lett.*, *33*, L24314, doi:10.1029/2006GL027890.

Tommasi, A., B. Tikoff, and A. Vauchez (1999), Upper mantle tectonics: Three-dimensional deformation, olivine crystallographic fabrics and seismic properties, Earth Planet. *Sci. Lett.*, *168*, 173–186, doi:10.1016/S0012-821X(99)00046-1.

Vauchez, A., A. Tommasi, and D. Mainprice (2012), Faults (shear zones) in the Earth's mantle, *Tectonophysics*, *558–559*, 1–27, doi:10.1016/j.tecto.2012.06.006.

Walker, K. T., A. A. Nyblade, S. L. Klemperer, G. H. R. Bokelmann, and T. J. Owens (2004), On the relationship between extension and anisotropy: Constraints from shear wave splitting across the East African Plateau, *J. Geophys. Res.*, *109*, B08302, doi:10.1029/2003JB002866.

Wdowinski, S., Y. Bock, G. Baer, L. Prawirodirdjo, N. Bechor, S. Naaman, R. Knafo, Y. Forrai, and Y. Melzer (2004), GPS measurements of current crustal movements along the Dead Sea Transform fault, *J. Geophys. Res.*, *109*, B05403, doi:10.1029/2003JB002640.

Weber, M., et al. (2009), Anatomy of the Dead Sea Transform from lithospheric to microscopic scale, *Rev. Geophys.*, *47*, RG2002, doi:10.1029/2008RG000264.

Wessel, P., and W. Smith (1991), Free software helps maps and display data, *Eos Trans. AGU*, *72*, 441.

van der Woerd, J., Y. Klinger, K. Sieh, P. Tapponnier, F. J. Ryerson, and A.-S. Meriaux (2006), Long-term slip rate of the southern San Andreas Fault from 10Be-26Al surface exposure dating of an offset alluvial fan, *J. Geophys. Res.*, *111*, B04407, doi:10.1029/2004JB003559.

Wüstefeld, A., and G. Bokelmann (2007), Null detection in shear-wave splitting measurements, *Bull. Seismol. Soc. Am.*, *97*, 1204–1211.